Beam current monitors

J.-C. Denard
Synchrotron SOLEIL, Saint-Aubin, France

Abstract
The instruments for monitoring charged particle beam current in accelerators are reviewed. After a description of the electromagnetic phenomena, we address the main design issues that a beam diagnostic engineer needs to know for implementing beam current monitors. Many current monitors are commercially available; however, choosing and implementing them properly is not always straightforward. Faraday cups, Wall Current Monitors (WCM), current transformers, and Direct-Current Current Transformers (DCCT) are described.

1 Introduction

Generally, the intensity, or charge, needs to be monitored in all accelerators. The wide range of accelerator types makes this a challenging task. The current can be simply the useful quantity in itself, but often it is an intermediary for measuring beam lifetime or for machine safety systems in storage rings, superconducting Linacs, and ERLs. The main kinds of current monitors such as Faraday cups, beam current transformers, and cavity monitors will be discussed.

2 Electromagnetic field associated to a particle beam

Apart from synchrotron radiation, the main electromagnetic field (EM field) used for current monitoring is the TEM field associated to charged particle beams. It is the subject of this section. A static punctual charge inside a long conducting tube generates an electric field, E, as shown in Fig. 1(a) [1, 2]. Its longitudinal distribution vanishes at distances that are several times that of the beam pipe radius a. The rms length of the distribution on the inner conducting pipe wall is [3, 4]:

$$\sigma_w = \frac{a}{\sqrt{2}} \ . \qquad (1)$$

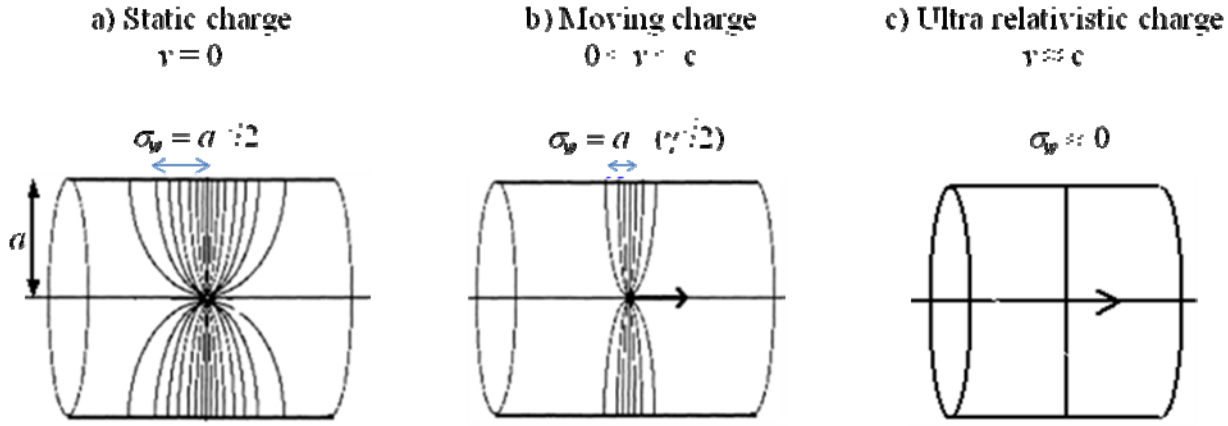

Fig. 1: Electric field lines generated by a punctual charge in a long circular tube

Charges in an accelerator are moving and the longitudinal extent of their electric field shrinks by the Lorentz factor γ [Fig. 1(b)]:

$$\gamma = \frac{1}{\sqrt{1 - v^2/c^2}} \ , \tag{2}$$

where v is the speed of the charge and c the speed of light.

Then the rms length of the field distribution on the conducting pipe wall becomes

$$\sigma_w = \frac{a}{\gamma\sqrt{2}} \ . \tag{3}$$

Most beam current monitors for accelerators measure highly relativistic particle beams, and the length σ_q of the electromagnetic field associated to a single particle is reduced to much less than the bunch length. Then, the electric field associated to a bunched beam of rms length σ_l moving at a highly relativistic speed in a conducting tube of radius a reproduces the longitudinal distribution of the beam (Fig. 2) provided that

$$\sigma_l >> a/\gamma\sqrt{2} \ . \tag{4}$$

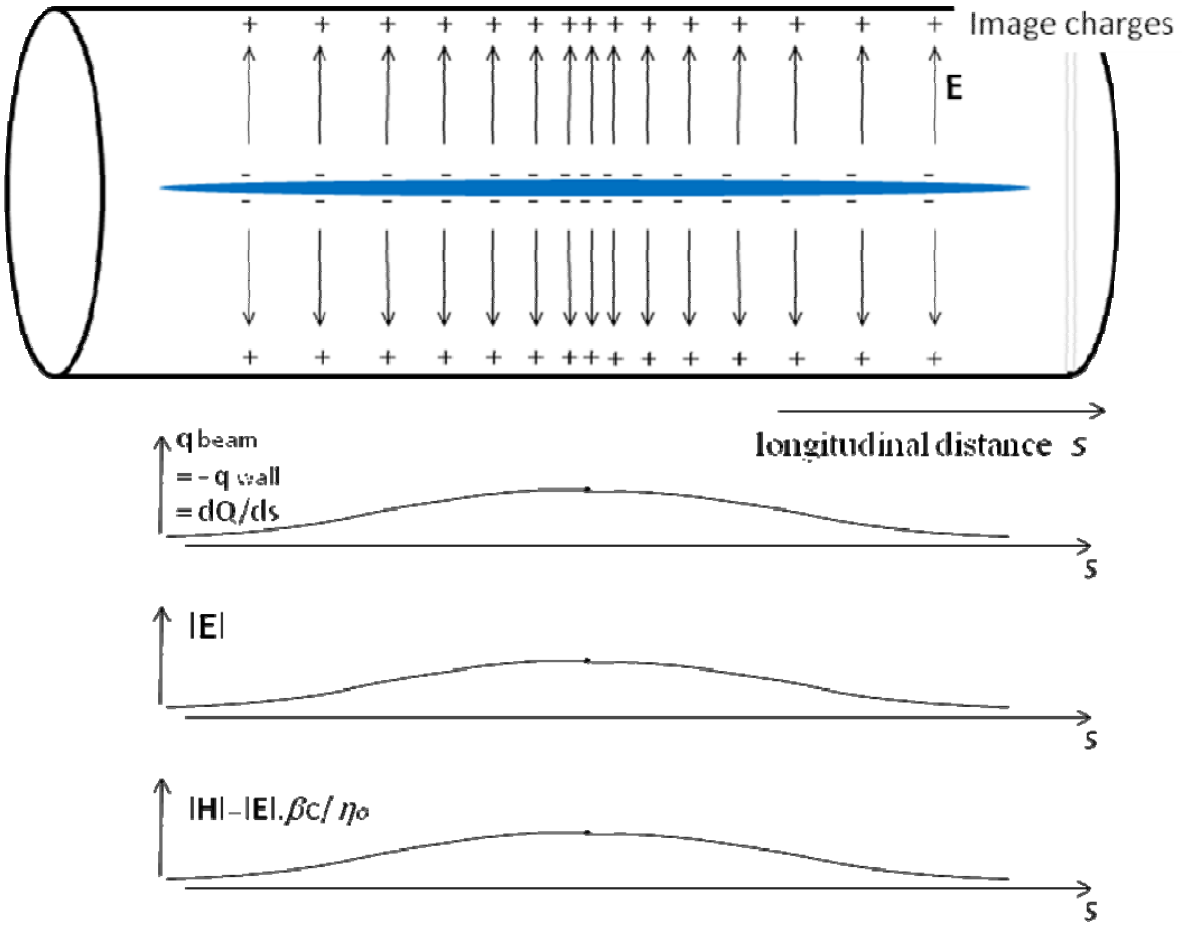

Fig. 2: Image charges, electric field, and magnetic fields associated to a charged particle beam for a beam length $\sigma_l >> a/\gamma\sqrt{2}$. Note that for a long beam, the electric field is constant for any β.

Let us look at the electric field associated to a slice of a beam much longer than $a/\gamma\sqrt{2}$. Whether or not the beam is moving, its associated electric field is radial as shown in Fig. 3. For any beam position and tube cross-section, the electric field is completely defined by Gauss's law:

$$\oint_S E \,.\, dA = \frac{Q_S}{\varepsilon_0} \quad . \tag{5}$$

Here, E is the electric field (in V/m), dA an element of the surface S (in m^2) enclosing the charge Q_S (in C) and ε_0 the permittivity of vacuum (in F/m).

This is a conservation law stating that the flux of E through the surface enclosing a volume is equal to the charge enclosed inside that same volume. It is much simpler if our long beam is centred in the tube. Then at any distance r from the beam axis, $\oint_S E \,.\, dA = 2\pi r \, \boldsymbol{E} \,.\, d\boldsymbol{l}$ and $Q_S = q\ dl$ with dq the charge density in C/m. Then the electric field at any radius r outside the beam but inside the tube is

$$|E|(r) = \frac{q}{2\pi r \varepsilon_0} \quad . \tag{6}$$

A few useful properties can be derived from Gauss's law. Since the tube is made of conducting material, there is no electric field inside its wall. No field in the longitudinal direction of the wall makes the electric field lines fall perpendicular to its surface. The electric field through the wall in the radial direction needs to be cancelled by opposite charges appearing on the inner wall surface. They are called image charges. Then, Gauss's law, applied to a volume enclosing the whole tube (the tube needs to be much longer than the beam), shows there is no electric field outside the tube since the total charge in the volume is zero.

The image charges distribute themselves in order to cancel the electric field inside the wall. The total image charge is opposite and equal to the absolute value of the free charge inside the tube. If the free charge moves, its image charge will move in the same direction, creating a wall current. However, this wall current does not occur on the DC component of the beam spectrum. A DC beam generates a constant electric field and a constant magnetic field, but the image charges do not need to move in order to be in agreement with Gauss's law, and a constant magnetic field does not induce any wall current. There is no DC wall current associated to the DC component of particle beams.

By definition, a charge moving longitudinally along the tube represents a current whose intensity is equal to the rate of charge flow past a given point:

$$i = dQ/dt \quad . \tag{7}$$

A charged particle beam moving at a speed $v = \beta c$ has an instantaneous intensity

$$i_b = q\ \beta c \tag{8}$$

with q the linear charge density in C/m and c the speed of light.

In the transverse plane, the current i_b generates a magnetic field H [Fig. 3(b)] perpendicular to the electric field and that follows Ampere's law:

$$\oint H \,.\, dl = i_b \quad . \tag{9}$$

There is a simple solution to Eq. (9) for a beam on axis in a circular tube:

$$|H|(r) = \frac{i_b}{2\pi r} = \frac{q\beta c}{2\pi r} . \tag{10}$$

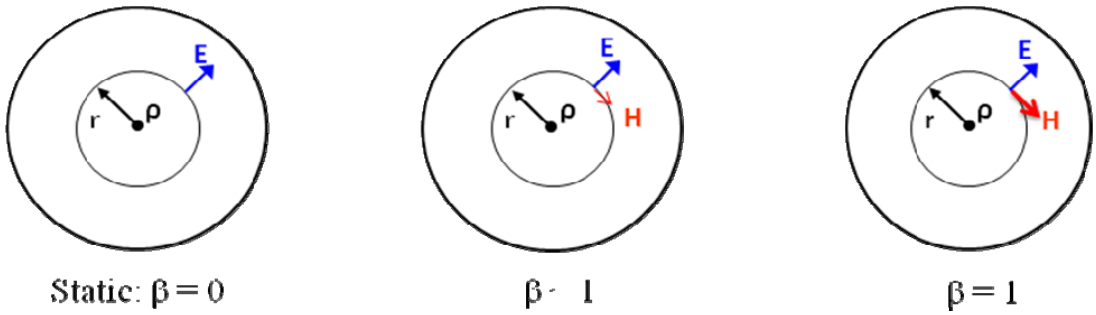

Fig. 3: Electric and magnetic fields in a beam 'slice' at different particle speeds

From Eqs. (6) and (10), one obtains the ratio between the electric and magnetic fields for ultrarelativistic beams:

$$\frac{|E|}{|H|} = \eta_0 = 377\ \Omega\ , \tag{11}$$

where η_0 is the impedance of free space (or vacuum) and can be expressed with vacuum permeability, μ_0, permittivity, ε_0, and speed of light c:

$$\eta_0 = \sqrt{\frac{\mu_0}{\varepsilon_0}} = \mu_0 c = \frac{1}{\varepsilon_0 c}\ . \tag{12}$$

These properties correspond to a Transverse electromagnetic (TEM) wave that propagates in vacuum at the speed of light in the beam direction. It is very similar to the TEM field associated to a signal propagating on a coaxial transmission line with air dielectric. Although the TEM wave propagation still exists at high frequencies, it is contaminated by the waveguide propagating modes that may occur above the cut off frequency f_c of the tube. For a cylindrical tube:

$$f_c = 2.405\ c/2\pi a\ . \tag{13}$$

Such parasitic modes become a problem when a monitor is located near a tube discontinuity where very short bunches launch strong wake fields that propagate in waveguide modes. Actually, the TEM wave propagation model is also true for any transverse beam position and tube cross-section as long as the beam is ultrarelativistic. The wall current that flows in the vacuum chamber wall is proportional to the electric field that falls on the surface of the wall minus its DC component.

Ampere's law enables us to calculate the magnetic field outside the tube. The wall current cancels the beam current inside a closed path around the tube, apart for the DC component. There is only a DC magnetic field outside the tube. It can be used for DC current monitoring.

Because of the similarities noted above between a bunched beam in a vacuum tube and pulsed currents in an air-filled coaxial line structure, it is very convenient to test beam current monitors on such coaxial structures. The behaviour at frequencies above the waveguide propagation cut-off is not identical, but it is located in a part of the spectrum that should be avoided.

3 Destructive monitors: Faraday cups

A Faraday cup is a piece of conducting material that collects all particles at the end of an accelerator. It intercepts the beam, but small cups can be retracted after a measurement so that the beam can go through. The collected current is directly measured with an ammeter for DC current measurements (Fig. 4) or an oscilloscope for measuring a pulsed beam [5].

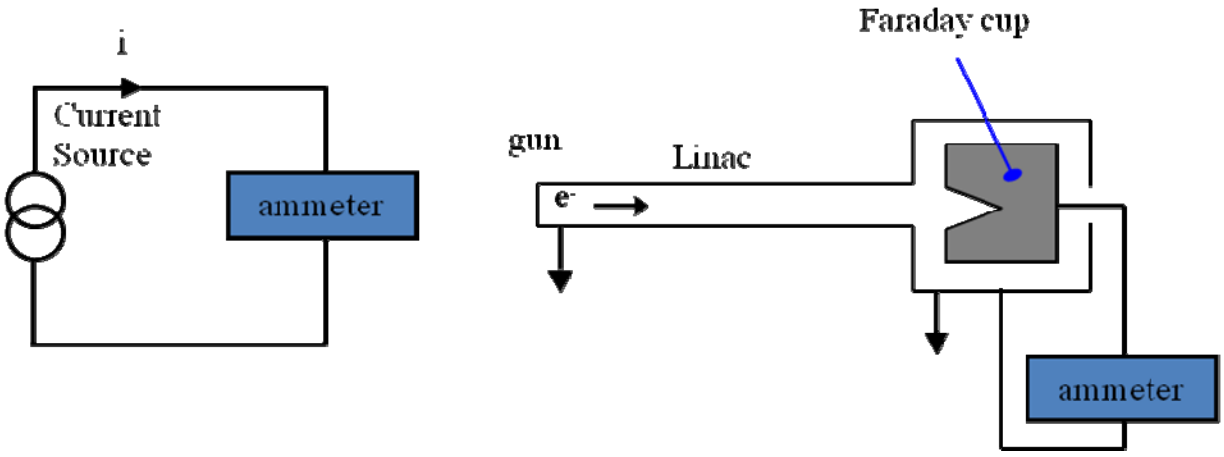

Fig 4: A Faraday cup is a simple way of measuring the beam current at the end of an accelerator

There are two kinds of charge that should not escape the cup: the backscattered particles and the electrons or positrons that may escape after multiple scattering in the cup. For beams of small transverse dimensions and good position stability, one can prevent most backscattered particles from exiting the cup with a narrow channel at the cup entrance. In addition, a bias voltage or magnetic field can be applied. Stopping most particles in the bulk of the cup depends on the type of particles, their energy, and the metal from which the cup is made. One centimetre of copper is enough for electrons below 1 MeV but up to one metre of lead becomes necessary for monitoring 6 GeV electrons with better than 1% absolute accuracy. For a given collecting efficiency, the higher the energy, the thicker the cup needs to be. Above 10– 20 MeV, the absorption of electrons in matter depends strongly on the radiation length of the material. This characteristic is shown in Table 1 [6] for several metals. When absolute accuracy is an issue, it is necessary to evaluate the collection efficiency with Monte Carlo codes such as EGGS4 developed at SLAC [7] or GEANT at CERN [8]. It is still a challenge to reach accuracies better than 1%.

Table 1: Radiation lengths of several metals

Material	Al	Fe	Cu	Ag	Pb	Au
Radiation length (cm)	8.9	1.76	1.44	0.85	0.56	0.33

The power of the spent beam can be an issue. A Faraday cup collecting a 5 MeV and 200 μA CW beam at JLab needs a 1 kW cooling circuit. Then the de-ionized cooling water and its hoses must be good insulators. Several gigohms are required for a 1 kV bias voltage in order to keep the absolute accuracy down to a few μA. Particle showers due to particles lost upstream and going through the hoses and water may deteriorate the insulation measured without beam and affect the measurement accuracy. Faraday cups need to be terminated by a DC circuit to avoid potentially dangerous high voltages that would develop at the cable end and provoke arcings.

It is possible to build a wide-bandwidth instrument for low-energy pulsed beams like at SLS (Fig. 5) thanks to a coaxial structure design [9]. The centre conductor collects the beam. The coaxial transmission line carries the beam-associated TEM wave spectrum through a 50 Ω vacuum feedthrough where a low-loss coaxial cable can be connected to a fast oscilloscope. The limitations of the coaxial design come with higher beam energies and average power. Above a few MeV it is difficult to collect all particles in a small piece of metal and cooling the cup would also seriously complicate the design.

Fig. 5: A wide-bandwidth retractable Faraday cup built at SLS

Calorimeters are another kind of destructive monitor for absolute beam current measurements. They consist in measuring the total energy delivered to a massive block of metal by measuring the temperature rise of the block after a known amount of beam energy has been spent in it. At high beam energies, a smaller quantity of metal is required to absorb the beam power than to absorb its charge. A calorimeter has been developed for the CEBAF CW beam [10].

4 Wall current monitors

Wall current monitors are mostly built for measuring beam longitudinal profiles when there is no synchrotron radiation: any Linacs or hadron circular accelerators. Whether or not it is relativistic, the wall current is representative of the beam image (minus the DC component) as long as relation (4) is fulfilled. The principle of a wall current monitor is simple; the wall current across a resistor gives rise to a measurable voltage (Fig. 6). That voltage is usually sent to a fast oscilloscope via a low-loss coaxial cable. Wall current has been described in Section 2. A typical beam, its wall current, and their respective spectra are shown in Fig. 7.

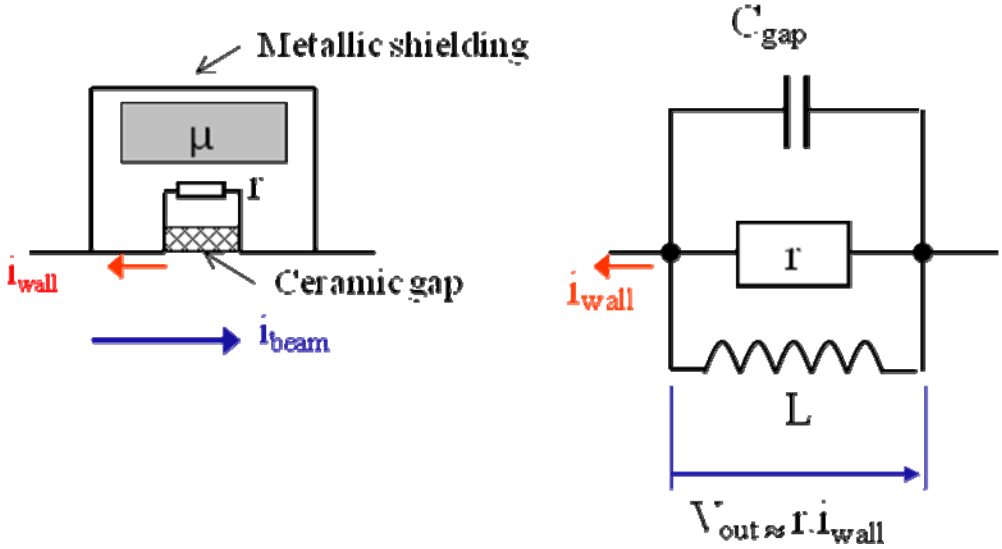

Fig. 6: Principle of wall current monitors

Like the beam itself, the wall current is an almost ideal current source with quasi-infinite internal impedance because its intensity does not change, whatever the wall impedance. The resistance *r* is a combination of several resistors connected in parallel. The challenge of wall current monitor

design is to keep the wall current spectrum in the high and low frequency domains. There is a self-inductance in series with a real resistor that limits the high-frequency bandwidth. Higher resistor values and smaller-sized resistors, preferably surface-mount devices, have higher frequency responses. The vacuum chamber conduction must be interrupted in order for the wall current to go through the resistors. It is usually done with a ceramic gap. The gap capacitor short-circuits the resistors at frequencies above f_{hf}:

$$f_{hf} = 1/(2\pi r C_{gap}) \,, \tag{14}$$

which usually limits the high-frequency response. At low frequencies, the resistors are short-circuited by miscellaneous vacuum chamber ground connections on each side of the gap. Electric shielding prevents parasitic external currents from flowing through r. It also prevents the monitor from becoming a wide-bandwidth broadcasting station. The low-frequency cut-off is

$$f_{lf} = r/(2\pi L) \,, \tag{15}$$

where L is

$$L = \frac{\mu_0 \mu_r}{2\pi} h \,\mathrm{Ln}(b/a) \,. \tag{16}$$

Here, μ_0 is the permeability of vacuum; μ_r the relative permeability of the toroid material; h, a and b the length, inner, and outer toroid diameter, respectively; and r the resistor. Actually, the same formula applies without magnetic material: then $\mu_r = 1$; h, a and b are the dimensions of the space between vacuum chamber and shielding. Since magnetic permeability above 10 000 is common, the advantage of magnetic material is obvious.

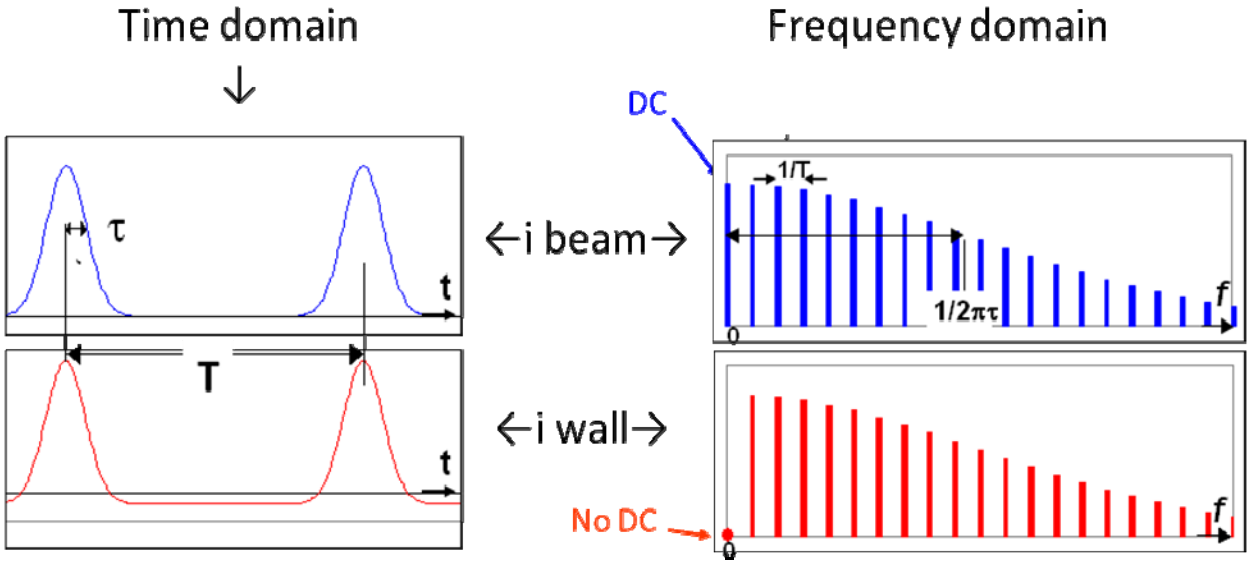

Fig. 7: Time and frequency domain representations of a periodic bunch beam

At not so high frequencies, (f > 300 MHz for a 100 mm diameter vacuum chamber) the wall current is not uniform for off-centred beams and it is necessary to properly combine the signals around the vacuum pipe. Solutions to this problem, and others, regarding very wide bandwidth wall current monitors can be found in Refs. [11, 12]. For low and mid range frequencies, one can consider a wall current monitor as a current transformer (see next section) with a one-turn secondary circuit connected to the resistor. Explanations on Fourier transforms and beam spectra can be found in Refs. [2, 13, and 14].

5 Beam current transformer

5.1 Principle of the beam current transformer

Although both electric and magnetic fields are present with charged particle beams, the magnetic field is the most commonly used in beam current monitors. Capacitive electrodes lack the low-frequency response that is important for current monitoring. Using the magnetic field, current transformers benefit from high permeability values (μ_r) available with magnetic materials. The DC component of the beam cannot be measured directly with a transformer. Transformers are AC beam current monitors. The transformer principle as well as valuable information on beam current transformers can be found in Refs. [15, 16].

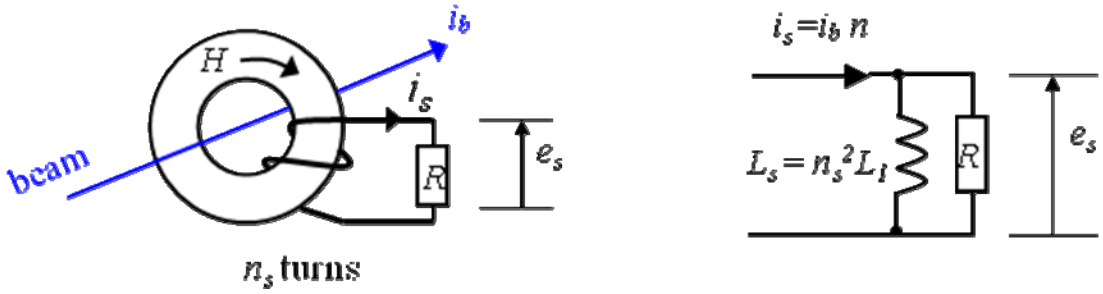

Fig. 8: Transformer and simplified equivalent circuit

The voltage e_s that develops on an n_s-turn winding (Fig. 8) is related to the variation of the total magnetic flux in the magnetic core by Faraday's law:

$$e_s = n_s \frac{d\Phi_T}{dt} = R\, i_s \ . \tag{17}$$

The contribution of the beam current to the total flux through the toroid cross-section is

$$\Phi_b = \int \mu_0 \mu_r H.dS = i_b \ (\mu_0 \mu_r \frac{h}{2\pi} \mathrm{Ln} \frac{b}{a}) \ . \tag{18}$$

Let us emphasize an important point: at low and mid frequencies, the beam's magnetic flux is concentrated in the toroid, and Ampere's law guarantees that the total flux is independent of the beam position. This is an advantage common to all beam current transformers.

The secondary circuit has several turns, each one contributing to the total flux. The contribution of the secondary winding to the total flux is

$$\Phi_s = \int \mu_0 \mu_r H.dS = n_s i_s \ (\mu_0 \mu_r \frac{h}{2\pi} \mathrm{Ln} \frac{b}{a}) \ . \tag{19}$$

The comparison of Eqs. (18) and (19) indicates that the beam current contribution to the total flux is that of a one-turn winding. It is interesting to define the self-inductance L_s of the n_s-turn winding. The self-induced voltage across an inductor by its varying current is

$$e_s = L_s \frac{di_s}{dt} \ . \tag{20}$$

Faraday's law on the winding alone ($i_b = 0$,) provides another expression of e_s:

$$e_s = n_s \frac{d\Phi_s}{dt} \ . \tag{21}$$

Combining Eqs. (20) and (21) leads to the inductance of the winding itself:

$$L_s = \frac{n_s \Phi_s}{i_s} \ . \tag{22}$$

Replacing Φ_s by its value in Eq. (19) yields

$$L_s = n_s^{\,2} \, \mu_0 \mu_r \frac{h}{2\pi} \mathrm{Ln} \frac{b}{a} = n_s^{\,2} L_1 \ . \tag{23}$$

Here L_1 is the inductance of one turn around the toroid ($n = 1$). It is equal to the term in parentheses in Eqs. (18) and (19). Then the total magnetic flux is

$$\Phi_T = \Phi_b + \Phi_s = L_1 (i_b + n_s i_s) \ . \tag{24}$$

This equation and Eq. (17) can be written with the Laplace formalism:

$$\Phi_T = L_1 (i_b + n_s i_s) \ , \tag{25}$$

$$s\Phi_T = \frac{R\, i_s}{n_s} \ . \tag{26}$$

Introducing $\tau = L_s/R$, the response to beam current is

$$i_s = \frac{i_b}{n_s} \frac{s\tau}{1 + s\tau} \ , \tag{27}$$

where τ is the time constant that limits the response in the low-frequency range. The equivalent circuit is shown in Fig. 8. The low-frequency cut-off is

$$f_{lf} = \frac{1}{2\pi\tau} = \frac{R}{2\pi L_s} \ . \tag{28}$$

The response to a long Linac macropulse is shown in Fig. 9. The low-frequency cut-off results in a signal droop during the macropulse. The droop can be reduced by increasing the time constant L_s/R. This is not always easy to do. An active circuit with an extra winding, due to Hereward at CERN, improves the low-frequency cut-off, but not the signal/noise ratio in the low-frequency domain [5, 15].

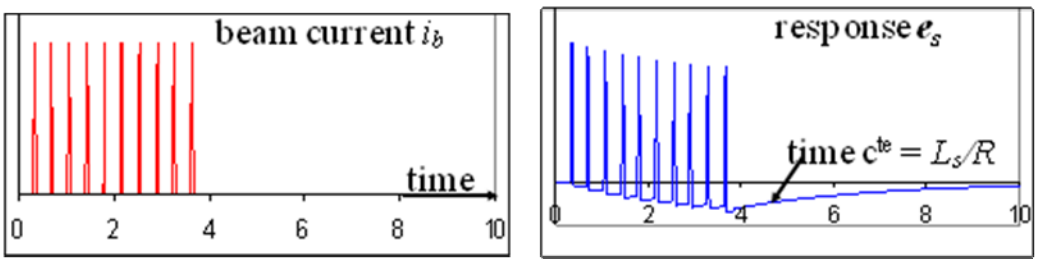

Fig. 9: Example of a Linac pulsed beam and current transformer response

In the mid-frequency range, the output signal e_s is

$$e_s = \frac{i_b}{n_s} R \ . \tag{29}$$

5.2 High-frequency issues

A number of elements limit the high-frequency response. An equivalent circuit of a current transformer is shown in Fig. 10. The outer shielding is actually a loop around the toroid. It is connected to the gap capacitance. It brings a capacitor C_{gap}/n_s^2 in parallel on the load. The winding capacity, not explicit on Fig. 10, is usually smaller than C_{gap}/n_s^2. Losses in the magnetic core due to eddy currents and magnetic material properties are represented by a resistance *Rc* in parallel on the secondary winding. *Rc* is a complex function of frequency.

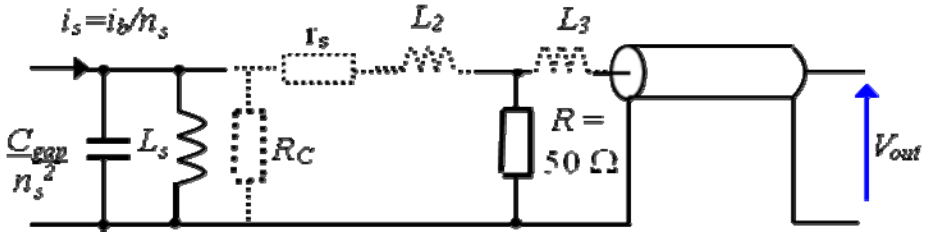

Fig. 10: High-frequency equivalent circuit of a beam current transformer. Stray elements are represented in dotted lines.

Series resistance r_s of the winding, inductance of the winding stray field L_2, and that of the coaxial cable connections become meaningful at high frequencies. Some resonances may need to be damped. For separating high-repetition bunches in accelerators like synchrotron light sources, the high-frequency response is needed. Fast current transformers with up to 1 GHz bandwidth are commercially available [17]. The gap needs to be wide enough to let the high-frequency components of the magnetic field reach the core. Most gap designs adopt a gap of at least one or two millimetres wide. In several machines, fast current transformers have been useless because of the influence of nearby pulsed magnets. These magnets as well as the monitor must be carefully shielded and grounded. On the SOLEIL Booster, a fast current transformer is installed two metres from a kicker magnet. These magnets with thousands of amperes and volts applied in very short times can spoil the relatively weak current monitor signal. An advantage of transformers is that both ends of the winding can be left floating. At the SOLEIL Booster and transport line, the signal is carried out with a triaxial cable as shown in Fig. 11. Other shielding and grounding techniques are detailed in Ref. [16].

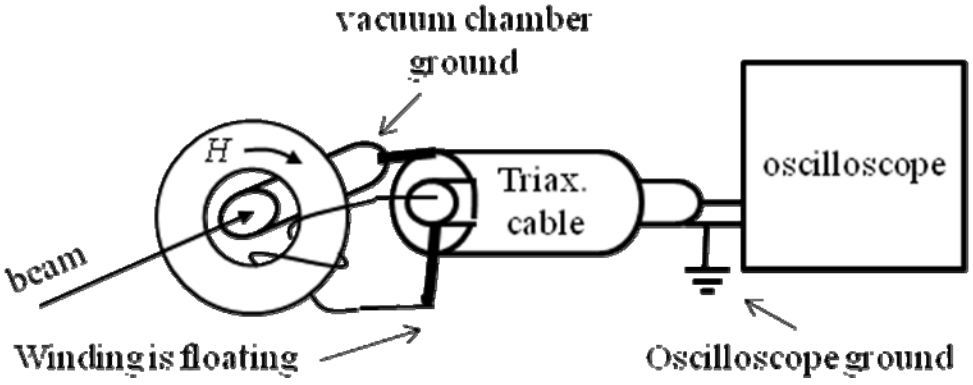

Fig. 11: Example of shielding and grounding

In order to keep the transformer bandwidth, the coaxial cable must be short and exhibit low losses.

5.3 Fast current transformers and high-current light sources

Fast transformers are very useful in many sections of accelerators [18]. However, for the high-current short-bunch light sources, the power absorbed by the toroid may induce excessive heat in its core. For a given bunch pattern, the total beam spectrum power is inversely proportional to the bunch length and proportional to the square of the average current. It is possible to add external capacitance in parallel with the gap at the cost of bandwidth reduction. Then adjacent bunches may not stay well separated from each other. The complete analysis of this problem during the design phase is quite complex and requires 3D electromagnetic simulation codes such as MAFIA [19] or GdFidl [20]. Another issue with the wide gap is its effect on beam stability. The same electromagnetic codes can estimate the wake field impedance. Another option for these machines is to use the synchrotron light they provide with a photodiode for relative measurement of the bunch filling pattern. The absolute current of individual bunches can be retrieved from the relative bunch filling pattern and a separate DC measurement of the total current. Non-destructive DC measurements are discussed in Section 5.5.

5.4 Integrating current transformer

On Linacs and transfer lines, it is interesting to monitor the charge of low-repetition-rate macropulses on several critical points in order to measure the transport efficiency. For this purpose, the high-frequency spectrum of a current transformer can be intentionally reduced and the time response becomes insensitive to pulse duration [21]. For example, the charge of all bunch patterns of Linac macropulses of a maximum length of 100 ns is measured with a low-pass filter of 1 µs time constant, which corresponds to a high-frequency cut-off reduced to f_{hf} = 160 kHz (Fig. 12). The low-frequency cut-off ($f_{lf} = R/2\pi L_s$), must be much lower in order to prevent any significant signal droop. There is no loss in the core at these frequencies and the monitor has a good absolute accuracy. An additional calibration loop on the toroid can even improve it further. The relatively slow signal eases the timing requirements of the digitization.

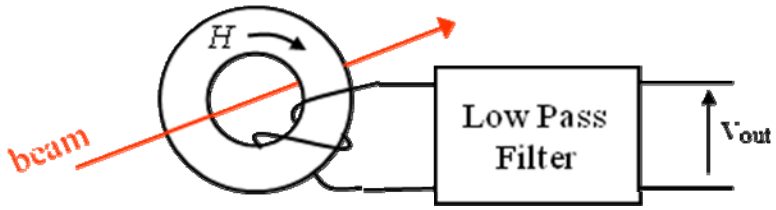

Fig. 12: The Integrating Current Transformer (ICT) for beam charge monitoring

5.5 Direct-Current Current Transformer (DCCT)

A major improvement in DC current monitoring has been brought by K. Unser with the implementation at CERN of a Direct-Current Current Transformer (DCCT) also called Parametric Current Transformer (PCT) [22]. It is the basis for accurate absolute measurements from DC to a few kHz with microampere accuracy [23]. The beam position does not affect the current measurement. The instrument needs a gap to avoid measuring stray currents in the vacuum pipe. Electric shielding will prevent the strong electromagnetic field developed across the gap from propagating outside.

The concept is to cancel the beam DC magnetic field with an external current precisely controlled via a feedback loop. A precision resistor in the feedback current path provides the output voltage. The zero magnetic field in a high permeability material is detected by driving it through saturation with a square symmetric AC current. A precision current source can be connected to a calibration winding in order to check the absolute accuracy.

Fortunately, accurate and carefully designed instruments are commercially available [17]. But the real performance of these expensive instruments is often spoiled by imperfect implementation. No varying external magnetic field should be allowed to reach the magnetic materials. This is done by

extensive magnetic shielding with iron and permalloy outside of the electric shielding. The instruments are very sensitive to temperature. For 1 μA long-term stability, it is necessary to stabilize the toroid temperature to the ± 0.1° level. This is a challenge for light sources since synchrotron radiation or wake fields passing through the gap may heat the toroid. Synchrotron radiation should be masked upstream of the monitor. The gap design requirement is different from the wide-bandwidth current monitors. It does not need to let high frequencies go through. A special seal, first designed by N. Rouvière at Saclay has a high capacitance and can be made for low wake-field losses. The seal is made of a thin capton foil sandwiched between two half aluminium VAT seals. Such seals have been successfully installed on the Elettra and SOLEIL storage ring (Fig. 13). At Elettra, the seal follows the vacuum chamber cross-section shape which is the best for minimizing wake-field losses but requires careful spacing and critical tightening of the seal. At SOLEIL, the seal is circular, but needs RF contact fingers to avoid heating from wake fields. The temperature at the seal location during vacuum chamber baking operations must not exceed 120°C. The toroid must also stay at a reasonable temperature during these periods. Both monitors have been working satisfactorily for several years.

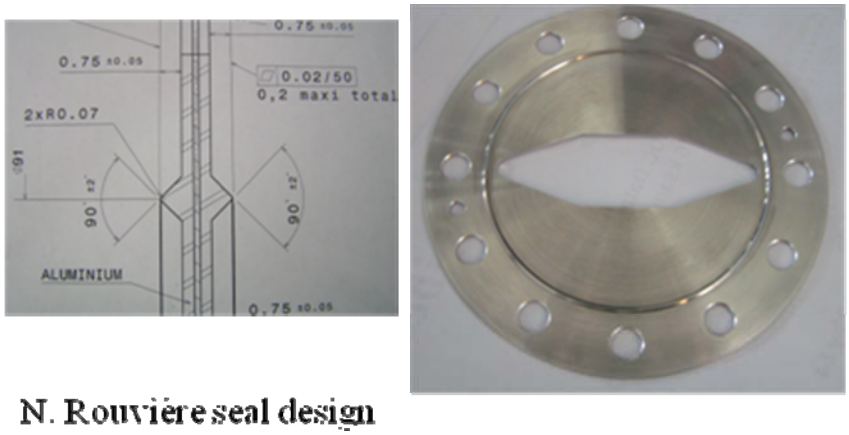

Fig. 13: SOLEIL custom-made ultravacuum seal for minimizing wake-field losses and heat on the DCCT toroid. Any heat reaching the toroid results in temperature rise that induces offset drifts.

Light sources do not usually have cylindrical vacuum chambers. An alternative solution to the custom-made seal, but that takes more longitudinal space on the machine, is to install a circular ceramic gap between two tapered transition from the gap and the rest of the machine. An external capacitance must be added in parallel on the gap in order to stop most of the AC electromagnetic power from the beam.

5.6 Monitors for low-intensity beams

For low currents, below 100 μA, the DCCT is not accurate enough. For these low currents, other solutions have been implemented. A. Peters developed a cryogenic current comparator for low-current ion beams at GSI [23]. Cavity monitors are also very sensitive but lack a good absolute accuracy. This can be solved by calibrating a cavity at higher currents with a DCCT or Faraday cup and using the linearity of the cavity for transposing the calibration at low currents.

5.6.1 Cryogenic current comparator

A cryogenic current comparator (CCC) like the DCCT is a null detector for the magnetic field. A Superconducting Quantum Interference Device (SQUID) detects extremely small magnetic fields. A resolution of a fraction of nA has been reached [24]. It provides a good absolute accuracy, independent of the beam position because of its use of the magnetic field, subject to Ampere's law.

5.6.2 Cavity current monitor

A cavity monitor makes use of the wall current that goes through the cavity impedance. The equivalent circuit of a cavity in its fundamental mode, like an accelerator cavity, is a parallel resonator [25]. High Q quality factors above 10 000 provide a large impedance at its resonant frequency. Cavity monitors are sensitive to nA beams but need an external calibration. The output pick-up voltage is proportional to the beam current. There is practically no beam position dependence in a cavity monitor. Numerical simulations show that its relative variations are less than 10^{-5} for beam offsets of 10% of the beam pipe diameter [26]. One may want to use stainless steel cavities for relatively low Q factors. In this way the resonant cavity drift with temperature is less important. An experiment requiring 0.1% absolute current measurements down to 1 μA at JLab has been instrumented with cavity monitors calibrated above 100 μA against a DDCT [26].

5.7 Photodiode current monitor

With the development of very sensitive and fast Avalanche Photodiodes (APD), there is an alternative solution to the FCTs for measuring the bunch filling pattern of light sources. A comparison between the two methods is shown in Fig. 14. Although the photodiode dynamic range is only of the order of 10 dB, it can monitor standard multibunch homogeneous fillings for top-up operations.

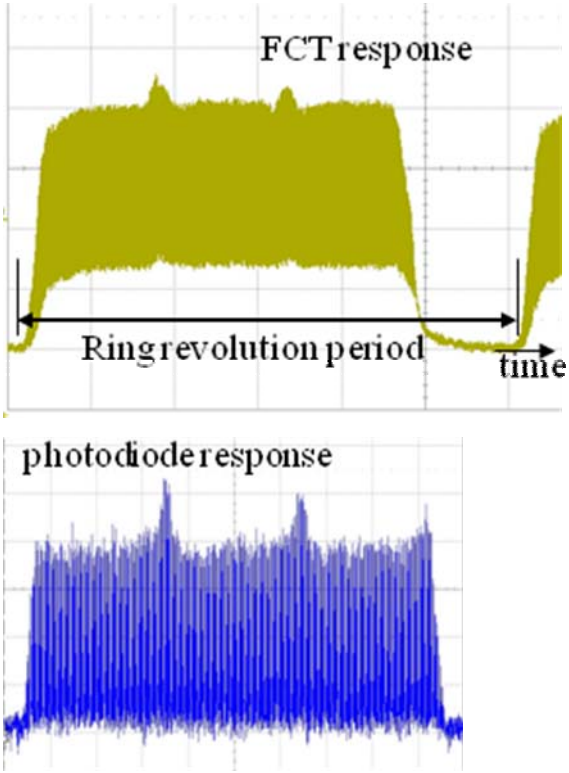

Fig. 14: A fast photodiode can provide the bunch filling pattern of a light source. On that example at SOLEIL, an APD shows a better separation between consecutive bunches than the FCT. However, the FCT has a 100 m low-loss cable going to the control room but the photodiode signal has been taken at the end of a short cable.

References

[1] E. Durand, *Electrostatique*, Tome II (Masson et Cie, Paris, 1966), p 381.

[2] A. Hofmann, Physical phenomena used in beam observation, *Third US–CERN School on Particle Accelerators: Frontiers of Particle Beams; Observation, Diagnosis and Correction*, Anacapri, Italy, 1988, M. Month and S. Turner (eds.) (Springer, Berlin, 1989), pp. 367–79 [Lecture Notes in Physics, 343].

[3] A. Hofmann and T. Risselada, *IEEE Trans. Nucl. Sci*., NS-30 n°4 (1983) 2400.
[4] A. Hofmann, Beam diagnostics, this CAS course.
[5] P. Strehl, Beam Instrumentation and Diagnostics (Springer Berlin, 2006); ISBN 978–3 540–26401-9.
[6] R. Jung, Beam intercepting monitors, *Third US–CERN School on Particle Accelerators: Frontiers of Particle Beams; Observation, Diagnosis and Correction*, Anacapri, Italy, 1988, M. Month and S. Turner (eds.) (Springer, Berlin, 1989), pp. 403–22 [Lecture Notes in Physics, 343].
[7] W.R. Nelson and D.W.O. Rogers, The EGS4 Code System, SLAC-265 (1985).
[8] H. Hirayama, GEANT4 collaboration *http://geant4.web.cern.ch/geant4/*
[9] M. Dach *et al*., SLS linac diagnostics–commissioning results, *Ninth Beam Instrumentation Workshop*, Cambridge, MA, 2000, R. C. Sibley and K. D. Jacobs (eds.) (AIP, New York, 2000), pp. 563–71 [AIP Conference Proceedings, 546].
[10] A. Freyberger, private communication.
[11] R. C. Weber, Longitudinal emittance: an introduction to the concept and survey of measurement techniques including design of a wall current monitor, *Accelerator Instrumentation*, *Proceedings of the First Annual Accelerator Instrumentation Workshop*, Upton, NY, 1989, E. R. Beadle and V. J. Castillo (eds.) (AIP, New York, 1990), pp. 85–126 [AIP Conference Proceedings, 212].
[12] P. Odier, A new wide band wall current monitor, *Sixth European Workshop on Beam Diagnostics and Instrumentation for Particle Accelerators,* Mainz, Germany, 2003, A. Peters and V. Schaa (eds.) (GSI, Darmstadt, 2003), p. 216.
[13] R. Littauer, Beam instrumentation, *Second Summer School on High-Energy Particle Accelerators: Physics of High-Energy Particle Accelerators*, Stanford, CA, 1982, M. Month (ed.) (AIP, New York, 1983), pp. 869–953 [AIP Conference Proceedings, 105].
[14] R. H. Siemann, Bunched beam diagnostics, *Physics of Particle Accelerators*, Fermilab Summer School 1987, Cornell Summer School 1988, M. Month and M. Dienes (eds.) [AIP Conference Proceedings, 184].
[15] R.C. Weber, Charged particle beam current monitoring tutorial, *Accelerator Instrumentation*, Sixth Beam Instrumentation Workshop, Vancouver, BC, 1994, G.H. MacKenzie *et al.* (eds.) (AIP, New York, 1995), pp. 3–23 [AIP Conference Proceedings, 333].
[16] R. C. Weber, Charged particle beam current monitoring tutorial, *Ninth Beam Instrumentation Workshop*, Cambridge, MA, 2000, K. D. Jacobs and R. C. Sibley (eds.) (AIP, New York, 2000) [AIP Conference Proceedings, 546].
[17] http://www.bergoz.com
[18] M. Kesselman, SNS project-wide beam current monitors, *Ninth Beam Instrumentation Workshop*, Cambridge, MA, 2000, K. D. Jacobs and R. C. Sibley (eds.) (AIP, New York, 2000) [AIP Conference Proceedings, 546].
[19] http://www.cst.com/Content/Products/MAFIA/Overview.aspx
[20] http://www.gdfidl.de
[21] K.B. Unser, Recent advances in beam current transformer technology and avenues for further developments, *Proceedings of the First European Workshop on Beam Diagnostics and Instrumentation for Particle Accelerators*, Montreux, Switzerland, 1993, C. Parthe (ed.), CERN SL/93–35 (BI), 1993, pp. 105–109.
[22] K.B. Unser, The parametric current transformer, a beam current monitor developed for LEP, *Third Annual Workshop on Accelerator Instrumentation*, Newport News, VI, 1991, W. Barry and P. K. Kloppel (eds.) (AIP, New York, 1991), pp. 266–75 [AIP Conference Proceedings, 252].
[23] W. Schutte and K. B. Unser, Beam current and beam lifetime measurements at the HERA proton storage ring, *Fourth Annual Workshop on Accelerator Instrumentation*, Berkeley, CA, 1992, J.A. Hinkson and G. Stover (eds.) (AIP, New York, 1993) [AIP Conference Proceedings, 281].
[24] A. Peters *et al*., A cryogenic current comparator for low intensity beams, *Proceedings of the First European Workshop on Beam Diagnostics and Instrumentation for Particle Accelerators*,

Montreux, Switzerland, 1993, C. Parthe (ed.), CERN PS/93–35 (BD), CERN SL/93–35 (BI), 1993.

[25] G.R. Lambertson, Electromagnetic detectors, *Third US–CERN School on Particle Accelerators: Frontiers of Particle Beams; Observation, Diagnosis and Correction*, Anacapri, Italy, 1988, M. Month and S. Turner (eds.) (Springer, Berlin, 1989), pp. 380–402 [Lecture Notes in Physics, 343].

[26] J.-C. Denard *et al*. High accuracy beam current monitor system for CEBAF's experimental hall A, *Particle Accelerator Conference*, Chicago, 2001, P. Lucas and S. Weber (eds.) (IEEE, Piscataway, NJ, 2001).